Wave transmission through two-dimensional structures by the hybrid FE/WFE approach

Giannoula Mitrou[a,*], Neil Ferguson[a], Jamil Renno[b]

[a] *Institute of Sound and Vibration Research*
University of Southampton, Southampton SO17 1BJ, UK
[b] *Plant Integrity Department, Doosan Babcock*
Porterfield Road, Renfrew PA4 8JD, UK

Abstract

The knowledge of the wave transmission and reflection characteristics in connected two-dimensional structures provides the necessary background for many engineering prediction methodologies. Extensive efforts have previously been exerted to investigate the propagation of waves in two-dimensional periodic structures. This work focuses on the analysis of the wave propagation and the scattering properties of joined structures comprising of two or more plates. The joint is modelled using the finite element (FE) method whereas each (of the joined) plate(s) is modelled using the wave and finite element (WFE) method. This latter approach is based on post-processing a standard FE model of a small segment of the plate using periodic structure theory; the FE model of the segment can be obtained using any commercial/in-house FE package. Stating the equilibrium and continuity conditions at the interfaces and expressing the motion in the plates in terms of the waves in each plate yield the reflection and transmission matrices of the joint. These can then be used to obtain the response of the whole structure, as well as investigating the frequency and incidence dependence for the flow of power in the system.

Keywords: wave propagation, reflection, transmission, power flow
2016 MSC: 00-01, 99-00

*Giannoula Mitrou
Email address: g.mitrou@soton.ac.uk (Giannoula Mitrou)
[1] InuTech GmbH, Fürther Strasse 212, 90403 Nürnberg, DE

1. Introduction

Wave methods are suitable for the analysis of the dynamic behaviour of simple structures, since they do not require powerful computing resources. This is very important for many applications especially at high frequencies where element-based models, e.g. the finite element (FE), become impractically large. The wave representation of the behaviour provides the necessary information for subsequent implementation of many techniques such as Power Flow Analysis, Statistical Energy Analysis (SEA)[1], Dynamical Energy Analysis (DEA) [2, 3], etc.

For simple cases such as slender connected beams, analytical solutions can be obtained for the reflection and transmission coefficients [4, 5]. However, developing analytical models that describe the dynamic behaviour of more complicated structures comprised of plates and different type of joints can be a very difficult task. Therefore, for such complicated structures, and particularly at high frequencies, the wave and finite element (WFE) method can be used. The WFE method for waveguides has been used to predict the free [6] and forced [7] response and to study different type of structures, such as thin-walled structures [8], laminated plates [6], fluid filled pipes [9, 10] etc. It has also been extended to two-dimensional plane [11, 12] and cylindrical structures [13]. An alternative formulation of the WFE method for two-dimensional structures is presented in [14], where a harmonic motion of the form $\exp(-\imath k_y y)$ was enforced in one direction, and the equation of motion is one-dimensionalised and subsequently solved using the WFE method of [6, 7].

The waves in two-dimensional systems such as plates are propagating at angle and when they are incident upon an interface they give rise to reflected and transmitted waves, which in general are propagating at a different angle in the transmitted system compared to the initial one. At first glance, the formulation of the WFE method which depends on the incident angle seems to be the most appropriate and general. This is also the formulation adopted in

this paper. Concerning the scattering properties of joints, wave approaches have been also used for the calculation of the reflection and transmission coefficients of plate/beam junctions [15], bolted joints [16] and curved beams [17]. The case of a junction with an elastic interlayer has been studied in [18], for a junction between semi-infinite plates [19, 20] and for junctions in heavyweight buildings. More recently, experimental work and numerical modelling of wave modes at a junction has been conducted [21, 22] using the analytical approach developed by Heron and Langley [15].

The hybrid FE/WFE approach for the computation of the scattering properties of joints in structures modelled as one-dimensional waveguides was first introduced in [23].

The objective of this article is to calculate the scattering properties of a joint in the case of two or three joined plates, that could represent a bonded joint, an L-shaped or a T-shaped junction. In section 2, a review of wave propagation in two-dimensional homogeneous structures and wave scattering upon a discontinuity is presented. In particular, the FE model and the free wave propagation in a segment of the plate is discussed. The knowledge of the wavemodes in combination with the scattering properties can be used to compute the energy flow of the waves as shown in subsection 2.6, through which the power reflection and transmission coefficients can be found, subsection 2.7. Section 3 is dedicated to the hybrid FE/WFE approach which yields the scattering matrix of the joint by applying continuity and equilibrium conditions at the interface nodes, for different cases of coupled plates. Section 4 includes some numerical results for the power scattering coefficients for different joint configurations, frequencies and incidence directions. The main results of the work are finally summarised in section 5.

2. A review of the WFE method for two-dimensional structures

In this section, the WFE method for two-dimensional structures is briefly reviewed.

2.1. Free wave propagation in two dimensions

Consider two-dimensional media which are homogeneous in both the x and y directions but whose properties may vary arbitrarily through its thickness in the z direction. Time harmonic motion of the form $\exp[\imath(\omega t - k_x x - k_y y)]$ and in the direction θ is assumed throughout this work where $k_x = k\cos\theta$ and $k_y = k\sin\theta$ are the components of the wavenumber k in the x and y directions. These wavenumbers might be real for propagating waves in the absence of damping, pure imaginary for evanescent waves or complex for oscillating, decaying waves.

2.2. The WFE model

The WFE method starts with a FE model of a small rectangular segment in the (x,y) plane of the plate with sides of lengths L_x and L_y as in Figure 1. This segment is meshed through the thickness using any number of elements. The only condition is that the nodes and degrees of freedom (dofs) are identically arranged on the opposite sides of the segment in order to relate the motion and the forces on each side of the segment in the propagating direction. Consequently, in the case of laminated plates any number of layers and any stacking sequence can be considered.

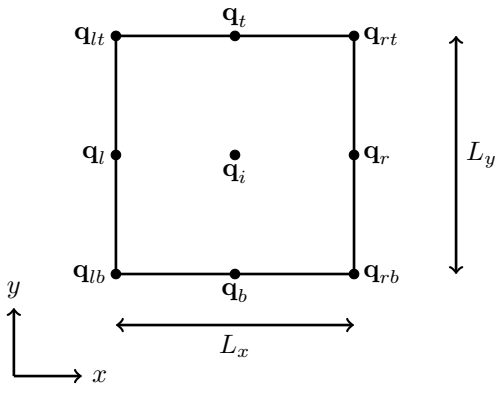

Figure 1: Rectangular segment for WFE method.

The vector $\mathbf{q}$ contains the generalised displacements at the left, right, top

and bottom sides and is partitioned as

$$\mathbf{q} = [\mathbf{q}_{lb}^T \quad \mathbf{q}_{rb}^T \quad \mathbf{q}_{lt}^T \quad \mathbf{q}_{rt}^T \quad \mathbf{q}_b^T \quad \mathbf{q}_r^T \quad \mathbf{q}_t^T \quad \mathbf{q}_l^T \quad \mathbf{q}_i^T]^T \ ,$$

where on each node there are m dofs. The vector of nodal forces $\mathbf{f}$ is partitioned in a similar manner.

2.3. Free wave propagation

If the structure undergoes time harmonic motion at frequency ω and in the absence of external forces, the nodal displacements and forces are related through the frequency dependent dynamic stiffness matrix of the segment

$$\mathbf{D}\mathbf{q} = \mathbf{f} \ , \tag{1}$$

where $\mathbf{D} = (\mathbf{K} + \imath\omega\mathbf{C} - \omega^2\mathbf{M})$ and $\mathbf{K}$, $\mathbf{C}$, and $\mathbf{M}$ are the stiffness, viscous damping and mass matrices, respectively. Imposing the wave propagation conditions in the y direction allows reduction of the dimension of Equation 1. Under the free passage of a wave whose wavenumber component in the y direction is specified as k_y, a transformation matrix $\mathbf{T}$ relates the full vector of dofs to a reduced set of dofs as

$$\mathbf{q} = \mathbf{T}\mathbf{q}_{red} \ , \quad \text{where} \quad \mathbf{q}_{red} = \begin{Bmatrix} \mathbf{q}_{lb} \\ \mathbf{q}_{rb} \\ \mathbf{q}_b \end{Bmatrix} = \begin{Bmatrix} \mathbf{q}_L \\ \mathbf{q}_R \\ \mathbf{q}_O \end{Bmatrix} \ .$$

The transformation matrix depends on the propagation constant $\lambda_y = e^{-\imath k_y L_y}$, which can relate the nodes on the top side of the segment and the middle nodes with those on the bottom side. Exploiting the periodicity assumption, other ways of reducing the matrices can be also applied. The transformation matrix

chosen for this analysis is written as:

$$\mathbf{T}(\lambda_y) = \begin{bmatrix} \mathbf{I} & \mathbf{0} & \mathbf{0} \\ \mathbf{0} & \mathbf{I} & \mathbf{0} \\ \lambda_y \mathbf{I} & \mathbf{0} & \mathbf{0} \\ \mathbf{0} & \lambda_y \mathbf{I} & \mathbf{0} \\ \mathbf{0} & \mathbf{0} & \mathbf{I} \\ \mathbf{0} & \lambda_y^{\frac{1}{2}} \mathbf{I} & \mathbf{0} \\ \mathbf{0} & \mathbf{0} & \lambda_y \mathbf{I} \\ \lambda_y^{\frac{1}{2}} \mathbf{I} & \mathbf{0} & \mathbf{0} \\ \mathbf{0} & \mathbf{0} & \lambda_y^{\frac{1}{2}} \mathbf{I} \end{bmatrix} .$$

Hence, Equation 1 can be written in terms of the reduced dofs as

$$\mathbf{T}^H (\mathbf{K} + \imath\omega\mathbf{C} - \omega^2 \mathbf{M}) \mathbf{T} \mathbf{q}_{red} = \mathbf{f}_{red} \ , \tag{2}$$

where H is the Hermitian matrix operator and

$$\mathbf{f}_{red} := \mathbf{T}^H \mathbf{f} = \begin{Bmatrix} \mathbf{f}_{lb} + \lambda_y^{-1} \mathbf{f}_{lt} + \lambda_y^{-\frac{1}{2}} \mathbf{f}_l \\ \mathbf{f}_{rb} + \lambda_y^{-1} \mathbf{f}_{rt} + \lambda_y^{-\frac{1}{2}} \mathbf{f}_r \\ \mathbf{f}_b + \lambda_y^{-1} \mathbf{f}_t + \lambda_y^{-\frac{1}{2}} \mathbf{f}_i \end{Bmatrix} = \begin{Bmatrix} \mathbf{f}_L \\ \mathbf{f}_R \\ \mathbf{f}_O \end{Bmatrix} .$$

Since the internal nodal forces are zero, $\mathbf{f}_i = \mathbf{0}$, and due to the equilibrium conditions on the bottom edge of the segment $\mathbf{f}_b + \lambda_y^{-1} \mathbf{f}_t = \mathbf{0}$ then the interior forces $\mathbf{f}_O = \mathbf{0}$.

Thus, Equation 2 can be expressed as

$$\widetilde{\mathbf{D}} \mathbf{q}_{red} = \mathbf{f}_{red} \ , \tag{3}$$

where $\widetilde{\mathbf{D}} = \mathbf{T}^H [\mathbf{K} + i\omega\mathbf{C} - \omega^2 \mathbf{M}] \mathbf{T}$; this can be rearranged into

$$\begin{bmatrix} \widetilde{\mathbf{D}}_{LL} & \widetilde{\mathbf{D}}_{LR} & \widetilde{\mathbf{D}}_{LO} \\ \widetilde{\mathbf{D}}_{RL} & \widetilde{\mathbf{D}}_{RR} & \widetilde{\mathbf{D}}_{RO} \\ \widetilde{\mathbf{D}}_{OL} & \widetilde{\mathbf{D}}_{OR} & \widetilde{\mathbf{D}}_{OO} \end{bmatrix} \begin{Bmatrix} \mathbf{q}_L \\ \mathbf{q}_R \\ \mathbf{q}_O \end{Bmatrix} = \begin{Bmatrix} \mathbf{f}_L \\ \mathbf{f}_R \\ \mathbf{0} \end{Bmatrix} . \tag{4}$$

Using the bottom nodes of Equation 4, the dofs in $\mathbf{q}_O$ can be eliminated, and the following form is obtained

$$\begin{bmatrix} \mathbf{D}_{LL} & \mathbf{D}_{LR} \\ \mathbf{D}_{RL} & \mathbf{D}_{RR} \end{bmatrix} \begin{Bmatrix} \mathbf{q}_L \\ \mathbf{q}_R \end{Bmatrix} = \begin{Bmatrix} \mathbf{f}_L \\ \mathbf{f}_R \end{Bmatrix} \ , \tag{5}$$

where

$$\begin{aligned} \mathbf{D}_{LL} &= \widetilde{\mathbf{D}}_{LL} - \widetilde{\mathbf{D}}_{LO}\widetilde{\mathbf{D}}_{OO}^{-1}\widetilde{\mathbf{D}}_{OL}, \quad & \mathbf{D}_{LR} &= \widetilde{\mathbf{D}}_{LR} - \widetilde{\mathbf{D}}_{LO}\widetilde{\mathbf{D}}_{OO}^{-1}\widetilde{\mathbf{D}}_{OR} \\ \mathbf{D}_{RL} &= \widetilde{\mathbf{D}}_{RL} - \widetilde{\mathbf{D}}_{RO}\widetilde{\mathbf{D}}_{OO}^{-1}\widetilde{\mathbf{D}}_{OL}, \quad & \mathbf{D}_{RR} &= \widetilde{\mathbf{D}}_{RR} - \widetilde{\mathbf{D}}_{RO}\widetilde{\mathbf{D}}_{OO}^{-1}\widetilde{\mathbf{D}}_{OR} \ . \end{aligned} \tag{6}$$

The system of Equation 5 is of size $2m \times 2m$, where m is the number of dofs at each corner or edge node of the segment, Figure 1. The formulation of Equation 5 is identical to the formulation of the WFE method for one-dimensional waveguides that was originally presented in [6].

2.4. Eigenvalue problem

Stating the periodicity and equilibrium conditions between the left and right edges of the segment, the admissible values of $\lambda_x = e^{-\imath k_x L_x}$ can be found by requiring

$$\mathbf{q}_R = \lambda_x \mathbf{q}_L \quad \text{and} \quad \lambda_x \mathbf{f}_L + \mathbf{f}_R = \mathbf{0} \ . \tag{7}$$

Substituting Equation 7 into Equation 5 yields an eigenvalue problem for the unknown wave constant λ_x

$$\mathscr{T} \begin{Bmatrix} \mathbf{q}_L \\ \mathbf{f}_L \end{Bmatrix} = \lambda_x \begin{Bmatrix} \mathbf{q}_L \\ \mathbf{f}_L \end{Bmatrix} \ , \tag{8}$$

where

$$\mathscr{T} = \begin{bmatrix} -\mathbf{D}_{LR}^{-1}\mathbf{D}_{LL} & \mathbf{D}_{LR}^{-1} \\ -\mathbf{D}_{RL} + \mathbf{D}_{RR}\mathbf{D}_{LR}^{-1}\mathbf{D}_{LL} & -\mathbf{D}_{RR}\mathbf{D}_{LR}^{-1} \end{bmatrix} \tag{9}$$

is the transfer matrix. For complicated structures with many dofs at each node, care needs to be taken when solving this eigenvalue problem as various numerical problems may arise [24]. The eigenvalue problem is usually then recast into one of a number of better-conditioned forms [25].

The solution of the eigenvalue problem in Equation 8 yields the propagation constants λ_x^j, $j = 1, \ldots, 2m$ and hence WFE estimates of the corresponding wavenumber k_x^j, $j = 1, \ldots, 2m$. Moreover, the eigenvectors of the eigenvalue problem correspond to the wavemode shapes $\boldsymbol{\phi}_j$, $j = 1, \ldots, 2m$ and contain information about both the nodal displacements $\mathbf{q}$ and the associated internal

forces $\mathbf{f}$ under the propagation of the j-th wave

$$\boldsymbol{\phi}_j = \begin{Bmatrix} \boldsymbol{\phi}_\mathbf{q} \\ \boldsymbol{\phi}_\mathbf{f} \end{Bmatrix}_j \quad , \quad j = 1, \ldots, 2m \ .$$

2.5. Wave basis

The transfer matrix is symplectic and the eigenvalues come in pairs and are of the form $\lambda_x^\pm = e^{\pm \imath k_x L_x}$, which represent positive and negative going wave pairs [25, 26]. Positive going waves are those for which the magnitude of the eigenvalues is less than 1, i.e. $|\lambda_x| < 1$ or if $|\lambda_x| = 1$, the power (energy flow) is positive, i.e.

$$\Re\{\mathbf{f}_L^T \dot{\mathbf{q}}_L\} = \Re\{\imath\omega \mathbf{f}_L^T \mathbf{q}_L\} = \Re\{\imath\omega \boldsymbol{\phi}_{\mathbf{f},\ell}^H \boldsymbol{\phi}_{\mathbf{q},\ell}\} > 0 \ . \tag{10}$$

With the positive and negative going waves identified, one can group the wavemodes as

$$\boldsymbol{\Phi} = \begin{bmatrix} \boldsymbol{\Phi}_\mathbf{q}^+ & \boldsymbol{\Phi}_\mathbf{q}^- \\ \boldsymbol{\Phi}_\mathbf{f}^+ & \boldsymbol{\Phi}_\mathbf{f}^- \end{bmatrix} . \tag{11}$$

The vectors $\mathbf{q}$ and $\mathbf{f}$ can be written as a linear combination of the eigenvectors with the amplitudes $\mathbf{a}^\pm$ as the coefficients of the linear combination; specifically

$$\mathbf{q} = \boldsymbol{\Phi}_\mathbf{q}^+ \mathbf{a}^+ + \boldsymbol{\Phi}_\mathbf{q}^- \mathbf{a}^- \quad , \quad \mathbf{f} = \boldsymbol{\Phi}_\mathbf{f}^+ \mathbf{a}^+ + \boldsymbol{\Phi}_\mathbf{f}^- \mathbf{a}^- \ . \tag{12}$$

The matrix $\boldsymbol{\Phi}$ defines a transformation between the physical domain, where the motion is described in terms of displacements and forces, i.e., $\mathbf{q}$ and $\mathbf{f}$, and the wave domain, where the motion is described in terms of wave amplitudes, $\mathbf{a}^\pm$ that travel in the positive and negative x directions, respectively.

Apart from solving the right eigenvalue problem of Equation 8, one can solve the left eigenvalue problem as well and compute the left eigenvectors. These are $1 \times 2m$ vectors which can be partitioned as:

$$\boldsymbol{\psi}_j = \begin{bmatrix} \boldsymbol{\psi}_\mathbf{q}^T & \boldsymbol{\psi}_\mathbf{f}^T \end{bmatrix}_j \ , \quad j = 1, \ldots, 2m \qquad \text{and} \qquad \boldsymbol{\Psi} = \begin{bmatrix} \boldsymbol{\Psi}_\mathbf{q}^+ & \boldsymbol{\Psi}_\mathbf{f}^+ \\ \boldsymbol{\Psi}_\mathbf{q}^- & \boldsymbol{\Psi}_\mathbf{f}^- \end{bmatrix} . \tag{13}$$

The left and the right eigenvectors are orthogonal and can be normalized so that

$$\boldsymbol{\Psi}\boldsymbol{\Phi} = \mathbf{I} \ . \tag{14}$$

The orthogonality relationships will be utilised in section 3 and section 4 to reduce numerical ill-conditioning.

2.6. Energy flow

The knowledge of the wavemodes can be further used to find the time averaged power [27] propagated by the waves as

$$\Pi = \frac{1}{2}\mathbf{a}^H \mathbf{P} \mathbf{a} \ ,$$

where $\mathbf{a} = [(\mathbf{a}^+)^T \ (\mathbf{a}^-)^T]^T$ is the vector of the wave amplitudes and $\mathbf{P}$ is the power matrix that can be expressed as

$$\mathbf{P} = \frac{i\omega}{2}\left\{ \begin{bmatrix} (\mathbf{\Phi}_\mathbf{q}^+)^H \mathbf{\Phi}_\mathbf{f}^+ & (\mathbf{\Phi}_\mathbf{q}^+)^H \mathbf{\Phi}_\mathbf{f}^- \\ (\mathbf{\Phi}_\mathbf{q}^-)^H \mathbf{\Phi}_\mathbf{f}^+ & (\mathbf{\Phi}_\mathbf{q}^-)^H \mathbf{\Phi}_\mathbf{f}^- \end{bmatrix} - \begin{bmatrix} (\mathbf{\Phi}_\mathbf{f}^+)^H \mathbf{\Phi}_\mathbf{q}^+ & (\mathbf{\Phi}_\mathbf{f}^+)^H \mathbf{\Phi}_\mathbf{q}^- \\ (\mathbf{\Phi}_\mathbf{f}^-)^H \mathbf{\Phi}_\mathbf{q}^+ & (\mathbf{\Phi}_\mathbf{f}^-)^H \mathbf{\Phi}_\mathbf{q}^- \end{bmatrix} \right\} . \tag{15}$$

The power matrix is Hermitian and thus the time averaged power Π is always real.

2.7. Scattering matrix

Structures can include discontinuities such as boundaries, line junctions or joints of finite dimensions, whose scattering properties are of a great importance for structural vibration analysis.

Consider a straight line junction between two plates as in Figure 2.

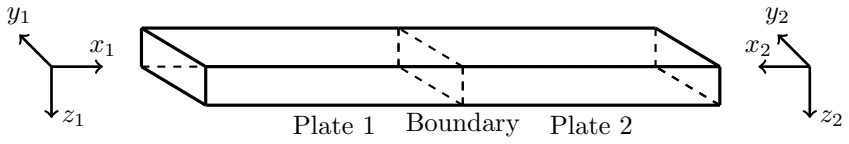

Figure 2: Two semi-infinite plates in the x direction are joined along the cross-sectional area.

Waves in "Plate 1" of amplitudes $\mathbf{a}_1^+$ are incident on the joint at an angle θ to the normal and they give rise to reflected waves of amplitudes $\mathbf{a}_1^- = \mathbf{r}_{11}\mathbf{a}_1^+$ and transmitted waves in "Plate 2" of amplitudes $\mathbf{a}_2^- = \mathbf{t}_{21}\mathbf{a}_1^+$, where $\mathbf{r}_{11}$ and

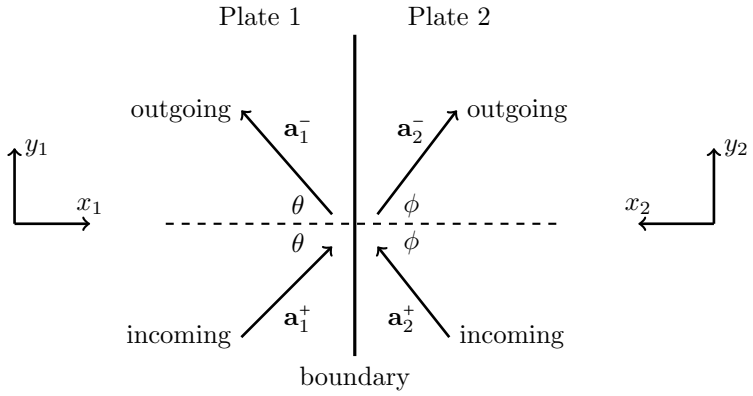

Figure 3: Reflection and transmission upon a joint and the coordinate conventions.

$\mathbf{t}_{21}$ are the matrices of the reflection and transmission coefficients of the joint, Figure 3.

These define the scattering matrix $\mathbf{s}$ of the joint, whose partitions relate the amplitudes of the incident and scattered waves as

$$\begin{Bmatrix} \mathbf{a}_1^- \\ \mathbf{a}_2^- \end{Bmatrix} = \mathbf{s} \begin{Bmatrix} \mathbf{a}_1^+ \\ \mathbf{a}_2^+ \end{Bmatrix} \quad \text{with} \quad \mathbf{s} = \begin{bmatrix} \mathbf{r}_{11} & \mathbf{t}_{12} \\ \mathbf{t}_{21} & \mathbf{r}_{22} \end{bmatrix} . \tag{16}$$

2.8. Reflection and transmission coefficients

Denoting by j the wavemodes and by $\mathbf{a}_j$ their related wave amplitude, from Equation 15, the power flow of the j-th wave is given by $\frac{1}{2}P_{jj}|\mathbf{a}_j|^2$. For an incoming wave denoted by j and by using the indices i and k for reflected and transmitted waves, respectively, the power reflection and transmission coefficients are computed by

$$\mathcal{R} = [R_{ij}] = \left[|r_{ij}|^2 \frac{P_{ii}}{P_{jj}} \right] \quad \text{and} \quad \mathcal{T} = [\mathcal{T}_{kj}] = \left[|t_{kj}|^2 \frac{P_{kk}}{P_{jj}} \right] . \tag{17}$$

For lossless systems the power scattering coefficients should sum to unity, i.e.,

$$\sum_i \mathcal{R}_{ij} + \sum_k \mathcal{T}_{kj} = 1 . \tag{18}$$

Note that this approach is applicable and indicates wave reflection and transmission when the waves are of different form, i.e., bending, shear, axial etc.

3. Hybrid FE/WFE approach

The approach developed in this article in order to compute the reflection and transmission properties in joined two-dimensional structures is the hybrid FE/WFE approach. The FE/WFE approach relies on modelling the plates by using the WFE method, as described in section 2, and on modelling a segment of the joint by using standard FE methods; the stiffness and mass matrices $\mathbf{K}^j$ and $\mathbf{M}^j$ are used to formulate the dynamic stiffness matrix of the joint

$$\mathbf{D}^j = \mathbf{K}^j - \omega^2 \mathbf{M}^j \ .$$

In principle, the scattering matrix is found by applying the equations of equilibrium and continuity at the interface nodes between the joints and the plates and by expressing the outgoing waves in the wave domain in terms of the incoming waves. For this purposes and for simplicity, it is also assumed that the interfaces have compatible meshes.

There are numerous possibilities of joining two or more plates together. The analysis for the computation of the scattering properties follows the type of joint under consideration. For the sake of simplicity, in the following sections the analysis is restricted to the joint. The general theory of the scattering properties of point joints and finite size joints in waveguide structures can be found in [14].

3.1. Joint along the common cross-sectional area

As shown in Figure 4, this type of joint is of finite size along the x direction but is extended infinitely in the y direction and all of its nodes defined on the edges are interface nodes between the joint and the plates. Note that there is no restriction here in the choice of the FE model for the joint, i.e. it can be plate or solid element, etc. The local coordinate system is defined such that the

x-axis points towards the direction of the joint. The rotation matrices $\mathbf{R_1}$ and $\mathbf{R_2}$ transform the dofs and the forces on "Plate 1" and "Plate 2" from the local coordinate system (x_1, y_1, z_1) and (x_2, y_2, z_2) to the global (X, Y, Z).

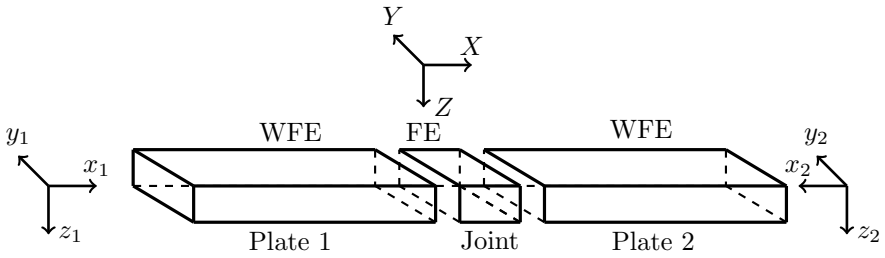

Figure 4: Two semi-infinite plates in the x direction and a joint with infinite length in the y direction and finite length in the x direction.

The time harmonic behaviour of the joint is described through the dynamic stiffness matrix $\mathbf{D}$, i.e.

$$\mathbf{D}^j \mathbf{Q}^j = \mathbf{F}^j, \tag{19}$$

where $\mathbf{Q}^j$ and $\mathbf{F}^j$ are the vectors of dofs and nodal forces on the joint.

Concatenating the relevant vectors and matrices for the individual plates, the vectors $\mathbf{Q}^j$ and $\mathbf{F}^j$ due to continuity and equilibrium conditions for the joint become:

$$\mathbf{Q}^j = \mathbf{R} \begin{Bmatrix} \mathbf{Q}^1 \\ \mathbf{Q}^2 \end{Bmatrix} \quad \text{and} \quad \mathbf{F}^j = \mathbf{R} \begin{Bmatrix} \mathbf{F}^1 \\ \mathbf{F}^2 \end{Bmatrix}, \tag{20}$$

where

$$\mathbf{R} = \begin{bmatrix} \mathbf{R_1} & \mathbf{0} \\ \mathbf{0} & \mathbf{R_2} \end{bmatrix} \tag{21}$$

is a block diagonal matrix, which includes the rotation matrices $\mathbf{R_1}$ and $\mathbf{R_2}$ for "Plate 1" and "Plate 2", respectively. The vectors $\mathbf{Q}^1$ and $\mathbf{Q}^2$ are their vector of displacements respectively. Equation 19 can be expressed in the wave domain in terms of the eigenvectors $\mathbf{\Phi}_{\mathbf{Q}}^{\{1,2\}\pm}$ and $\mathbf{\Phi}_{\mathbf{F}}^{\{1,2\}\pm}$ using Equation 12.

Combining Equation 12 with Equation 20, the dofs at the interface can be

rewritten in a matrix form as follows

$$\mathbf{Q}^j = \mathbf{R}\left[\mathbf{\Phi}_{\boldsymbol{Q}}^{in}\begin{Bmatrix}\mathbf{a}_1^+\\ \mathbf{a}_2^+\end{Bmatrix} + \mathbf{\Phi}_{\boldsymbol{Q}}^{out}\begin{Bmatrix}\mathbf{a}_1^-\\ \mathbf{a}_2^-\end{Bmatrix}\right], \tag{22}$$

where

$$\mathbf{\Phi}_{\boldsymbol{Q}}^{in} = \begin{bmatrix}\mathbf{\Phi}_{\mathbf{Q}}^{1+} & \mathbf{0}\\ \mathbf{0} & \mathbf{\Phi}_{\mathbf{Q}}^{2+}\end{bmatrix} \quad \text{and} \quad \mathbf{\Phi}_{\boldsymbol{Q}}^{out} = \begin{bmatrix}\mathbf{\Phi}_{\mathbf{Q}}^{1-} & \mathbf{0}\\ \mathbf{0} & \mathbf{\Phi}_{\mathbf{Q}}^{2-}\end{bmatrix}.$$

Similarly, the vector $\mathbf{F}^j$ is given by

$$\mathbf{F}^j = \mathbf{R}\left[\mathbf{\Phi}_{\boldsymbol{F}}^{in}\begin{Bmatrix}\mathbf{a}_1^+\\ \mathbf{a}_2^+\end{Bmatrix} + \mathbf{\Phi}_{\boldsymbol{F}}^{out}\begin{Bmatrix}\mathbf{a}_1^-\\ \mathbf{a}_2^-\end{Bmatrix}\right]. \tag{23}$$

The arrangement of the matrices in Equation 22 and Equation 23 is done with respect to the outgoing and incoming waves. Returning to the FE model of the joint and Equation 19, the latter is written

$$\mathbf{D}^j\mathbf{R}\left[\mathbf{\Phi}_{\boldsymbol{Q}}^{in}\begin{Bmatrix}\mathbf{a}_1^+\\ \mathbf{a}_2^+\end{Bmatrix} + \mathbf{\Phi}_{\boldsymbol{Q}}^{out}\begin{Bmatrix}\mathbf{a}_1^-\\ \mathbf{a}_2^-\end{Bmatrix}\right] = \mathbf{R}\left[\mathbf{\Phi}_{\boldsymbol{F}}^{in}\begin{Bmatrix}\mathbf{a}_1^+\\ \mathbf{a}_2^+\end{Bmatrix} + \mathbf{\Phi}_{\boldsymbol{F}}^{out}\begin{Bmatrix}\mathbf{a}_1^-\\ \mathbf{a}_2^-\end{Bmatrix}\right]. \tag{24}$$

Taking into account Equation 16 and rearranging Equation 24 in terms of incoming and outgoing waves

$$\left[\mathbf{D}^j\mathbf{R}\mathbf{\Phi}_{\boldsymbol{Q}}^{in} - \mathbf{R}\mathbf{\Phi}_{\boldsymbol{F}}^{in}\right]\begin{Bmatrix}\mathbf{a}_1^+\\ \mathbf{a}_2^+\end{Bmatrix} = \left[\mathbf{R}\mathbf{\Phi}_{\boldsymbol{F}}^{out} - \mathbf{D}^j\mathbf{R}\mathbf{\Phi}_{\boldsymbol{Q}}^{out}\right]\begin{Bmatrix}\mathbf{a}_1^-\\ \mathbf{a}_2^-\end{Bmatrix}, \tag{25}$$

the scattering matrix is finally given by

$$\mathbf{s} = -\left[\mathbf{D}^j\mathbf{R}\mathbf{\Phi}_{\boldsymbol{Q}}^{out} - \mathbf{R}\mathbf{\Phi}_{\boldsymbol{F}}^{out}\right]^{-1}\left[-\mathbf{R}\mathbf{\Phi}_{\boldsymbol{F}}^{in} + \mathbf{D}^j\mathbf{R}\mathbf{\Phi}_{\boldsymbol{Q}}^{in}\right]. \tag{26}$$

Since the inversion of the matrix in Equation 26 can cause numerical instabilities, appropriate use of the left eigenvector matrix $\mathbf{\Psi}$ from Equation 13 and the orthogonality conditions can remove these numerical difficulties [23]. Here one can premultiply with the $\mathbf{\Psi}_{\boldsymbol{Q}}^{out}$ matrix, which has the following form:

$$\mathbf{\Psi}_{\boldsymbol{Q}}^{out} = \begin{bmatrix}\mathbf{\Psi}_{\mathbf{Q}}^{1-} & \mathbf{0}\\ \mathbf{0} & \mathbf{\Psi}_{\mathbf{Q}}^{2-}\end{bmatrix}.$$

The scattering matrix finally takes the form

$$\mathbf{s} = -\left[\mathbf{\Psi}_{\boldsymbol{Q}}^{out}(\mathbf{D}^j\mathbf{R}\mathbf{\Phi}_{\boldsymbol{Q}}^{out} - \mathbf{R}\mathbf{\Phi}_{\boldsymbol{F}}^{out})\right]^{-1}\mathbf{\Psi}_{\boldsymbol{Q}}^{out}\left[-\mathbf{R}\mathbf{\Phi}_{\boldsymbol{F}}^{in} + \mathbf{D}^j\mathbf{R}\mathbf{\Phi}_{\boldsymbol{Q}}^{in}\right]. \tag{27}$$

3.2. Lap joint

Overlapped plates, see Figure 5, which can be found in an adhesive bonding type of connection, can be considered as another type of joint. In this case, the lap joint includes not only interface nodes but also non-interface ones, on which the external forces are equal to zero. The interface and the non-interface nodes are distinguished and denoted by n and i respectively.

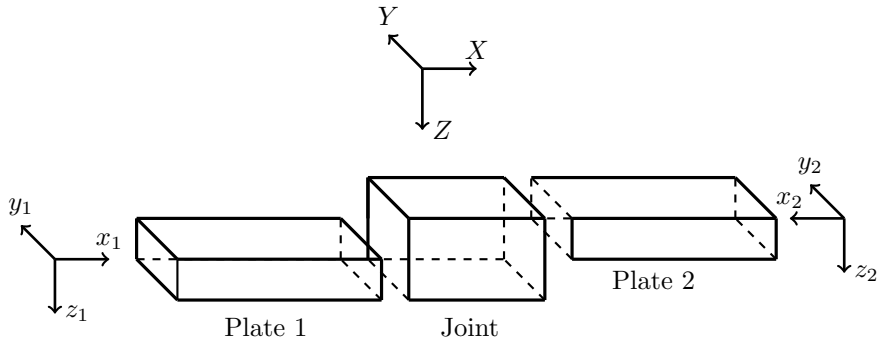

Figure 5: Two plates in an off-set.

After partitioning the dynamic stiffness matrix with respect to the interface and non-interface nodes, the time harmonic behaviour of the joint is described through

$$\widetilde{\mathbf{D}}^j \begin{Bmatrix} \mathbf{Q}_i^j \\ \mathbf{Q}_n^j \end{Bmatrix} \equiv \begin{bmatrix} \widetilde{\mathbf{D}}_{ii}^j & \widetilde{\mathbf{D}}_{in}^j \\ \widetilde{\mathbf{D}}_{ni}^j & \widetilde{\mathbf{D}}_{nn}^j \end{bmatrix} \begin{Bmatrix} \mathbf{Q}_i^j \\ \mathbf{Q}_n^j \end{Bmatrix} = \begin{Bmatrix} \mathbf{F}_i^j \\ \mathbf{F}_n^j \end{Bmatrix} , \tag{28}$$

Since no external forces are applied at the non-interface nodes, i.e., $\mathbf{F}_n^j = \mathbf{0}$, then Equation 28 reduces to

$$\mathbf{D}_{ii}^j \mathbf{Q}_i^j = \mathbf{F}_i^j \tag{29}$$

where

$$\mathbf{D}_{ii}^j = \widetilde{\mathbf{D}}_{ii}^j - \widetilde{\mathbf{D}}_{in}^j [\widetilde{\mathbf{D}}_{nn}^j]^{-1} \widetilde{\mathbf{D}}_{ni}^j, \quad \text{and} \quad \mathbf{Q}_n^j = -[\widetilde{\mathbf{D}}_{nn}^j]^{-1} \widetilde{\mathbf{D}}_{ni}^j \mathbf{Q}_i^j \ .$$

Similar to Equation 20, the vectors $\mathbf{Q}_i^j$ and $\mathbf{F}_i^j$ can be expressed in the wave domain with respect to "Plate 1" and "Plate 2".

The scattering matrix is given by

$$\mathbf{s} = -\left[\mathbf{D}_{ii}^{j}\mathbf{R}\boldsymbol{\Phi}_{\boldsymbol{Q}_i}^{out} - \mathbf{R}\boldsymbol{\Phi}_{\boldsymbol{F}_i}^{out}\right]^{-1}\left[-\mathbf{R}\boldsymbol{\Phi}_{\boldsymbol{F}_i}^{in} + \mathbf{D}_{ii}^{j}\mathbf{R}\boldsymbol{\Phi}_{\boldsymbol{Q}_i}^{in}\right] \tag{30}$$

and by the use of the $\boldsymbol{\Psi}_{\boldsymbol{Q}}^{out}$ matrix

$$\mathbf{s} = -\left[\boldsymbol{\Psi}_{\boldsymbol{Q}_i}^{out}(\mathbf{D}_{ii}^{j}\mathbf{R}\boldsymbol{\Phi}_{\boldsymbol{Q}_i}^{out} - \mathbf{R}\boldsymbol{\Phi}_{\boldsymbol{F}_i}^{out})\right]^{-1}\boldsymbol{\Psi}_{\boldsymbol{Q}_i}^{out}\left[-\mathbf{R}\boldsymbol{\Phi}_{\boldsymbol{F}_i}^{in} + \mathbf{D}^{j}\mathbf{R}\boldsymbol{\Phi}_{\boldsymbol{Q}_i}^{in}\right] . \tag{31}$$

3.3. L-shaped joint

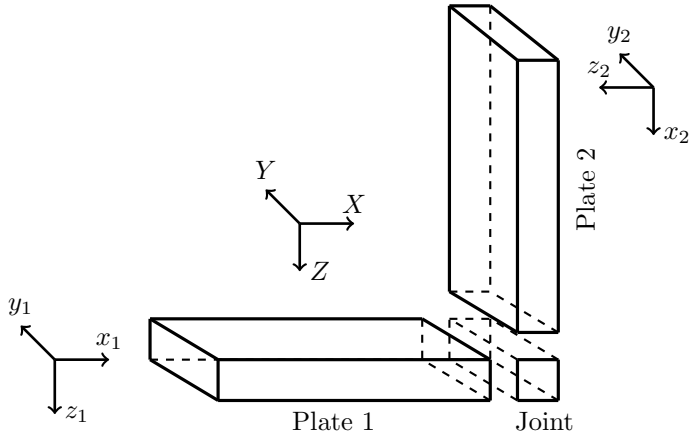

Figure 6: Two plates in a L-shaped joint.

Another type of connection includes semi-infinite plates formed with an angle between them. As an example one can consider two semi-infinite plates in a 90 degrees angle forming an L-shaped structure, see Figure 6. As for the off-set case, for this L-shaped joint the nodes on the joint can be first distinguished into interface and non-interface nodes. In contrast to the case of two plates in a line, in this case the interface nodes can also be common nodes in both plates, denoted by $\mathbf{Q}_c$, and nodes which belong to only one of the plates, denoted by $\mathbf{Q}_s = \begin{Bmatrix}\mathbf{Q}_s^1 \\ \mathbf{Q}_s^2\end{Bmatrix}$. The vectors of displacements and forces at the interface nodes can

be written as

$$\mathbf{Q}_i = \begin{Bmatrix} \mathbf{Q}_c \\ \mathbf{Q}_s^1 \\ \mathbf{Q}_s^2 \end{Bmatrix} , \qquad \text{and} \qquad \mathbf{F}_i = \begin{Bmatrix} \mathbf{F}_c \\ \mathbf{F}_s^1 \\ \mathbf{F}_s^2 \end{Bmatrix} .$$

The continuity conditions at the interface nodes which are common on both plates can be stated as

$$\mathbf{Q}_c = \mathbf{R}_1 \mathbf{Q}_c^1 = \mathbf{R}_2 \mathbf{Q}_c^2 , \tag{32}$$

where $\mathbf{R}_1$ and $\mathbf{R}_2$ are the rotation matrices of "Plate 1" and "Plate 2", since the continuity condition is expressed in the global coordinate system (X-Y-Z). Substituting $\mathbf{Q}_c^1$ and $\mathbf{Q}_c^2$ with their representation in the wave domain, Equation 32 is further written as

$$\mathbf{R}_1 \left[\mathbf{\Phi}_{\mathbf{Q}_c}^{1+} \mathbf{a}_1^+ + \mathbf{\Phi}_{\mathbf{Q}_c}^{1-} \mathbf{a}_1^- \right] = \mathbf{R}_2 \left[\mathbf{\Phi}_{\mathbf{Q}_c}^{2+} \mathbf{a}_2^+ + \mathbf{\Phi}_{\mathbf{Q}_c}^{2-} \mathbf{a}_2^- \right] .$$

Rearranging the latter with respect to incoming and outgoing waves, gives

$$\mathbf{\Phi}_c^{in} \begin{Bmatrix} \mathbf{a}_1^+ \\ \mathbf{a}_2^+ \end{Bmatrix} = \mathbf{\Phi}_c^{out} \begin{Bmatrix} \mathbf{a}_1^- \\ \mathbf{a}_2^- \end{Bmatrix} \tag{33}$$

where

$$\mathbf{\Phi}_c^{in} = \begin{bmatrix} \mathbf{R}_1 \mathbf{\Phi}_{\mathbf{Q}_c}^{1+} & -\mathbf{R}_2 \mathbf{\Phi}_{\mathbf{Q}_c}^{2+} \end{bmatrix} \qquad \text{and} \qquad \mathbf{\Phi}_c^{out} = \begin{bmatrix} \mathbf{R}_1 \mathbf{\Phi}_{\mathbf{Q}_c}^{1-} & -\mathbf{R}_2 \mathbf{\Phi}_{\mathbf{Q}_c}^{2-} \end{bmatrix} .$$

At the common nodes for the vector of nodal forces it holds

$$\mathbf{F}_c = \mathbf{R}_1 \mathbf{F}_c^1 + \mathbf{R}_2 \mathbf{F}_c^2 . \tag{34}$$

The equilibrium condition at the joint, expressed in the global coordinates system using Equation 29 can be stated as

$$\mathbf{D}_{ii}^j \mathbf{R}_q \begin{Bmatrix} \mathbf{Q}_c^1 \\ \mathbf{Q}_s^1 \\ \mathbf{Q}_s^2 \end{Bmatrix} = \mathbf{T}_r \mathbf{R}_f \begin{Bmatrix} \mathbf{F}_c^1 \\ \mathbf{F}_c^2 \\ \mathbf{F}_s^1 \\ \mathbf{F}_s^2 \end{Bmatrix} , \tag{35}$$

where $\mathbf{R}_q$ and $\mathbf{R}_f$ are block diagonal matrices including the rotation matrices $\mathbf{R}_1$ and $\mathbf{R}_2$, and $\mathbf{T}_r$ is a transformation matrix of the form

$$\mathbf{T}_r = \begin{bmatrix} \mathbf{I} & \mathbf{I} & \mathbf{0} & \mathbf{0} \\ \mathbf{0} & \mathbf{0} & \mathbf{I} & \mathbf{0} \\ \mathbf{0} & \mathbf{0} & \mathbf{0} & \mathbf{I} \end{bmatrix}$$

which is used to express the relation of Equation 34. As before, the vectors at the interface nodes are expressed in terms of wave amplitudes. The vector of displacements is written

$$\begin{Bmatrix} \mathbf{Q}_c^1 \\ \mathbf{Q}_s^1 \\ \mathbf{Q}_s^2 \end{Bmatrix} = \mathbf{\Phi}_{\boldsymbol{Q}}^{in} \begin{Bmatrix} \mathbf{a}_1^+ \\ \mathbf{a}_2^+ \end{Bmatrix} + \mathbf{\Phi}_{\boldsymbol{Q}}^{out} \begin{Bmatrix} \mathbf{a}_1^- \\ \mathbf{a}_2^- \end{Bmatrix} ,$$

where

$$\mathbf{\Phi}_{\boldsymbol{Q}}^{in} = \begin{bmatrix} \mathbf{\Phi}_{\boldsymbol{Q}_c}^{1+} & \mathbf{0} \\ \mathbf{\Phi}_{\boldsymbol{Q}_s}^{1+} & \mathbf{0} \\ \mathbf{0} & \mathbf{\Phi}_{\boldsymbol{Q}_s}^{2+} \end{bmatrix} \quad \text{and} \quad \mathbf{\Phi}_{\boldsymbol{Q}}^{out} = \begin{bmatrix} \mathbf{\Phi}_{\boldsymbol{Q}_c}^{1-} & \mathbf{0} \\ \mathbf{\Phi}_{\boldsymbol{Q}_s}^{1-} & \mathbf{0} \\ \mathbf{0} & \mathbf{\Phi}_{\boldsymbol{Q}_s}^{2-} \end{bmatrix} .$$

The vector of forces is respectively of the form

$$\begin{Bmatrix} \mathbf{F}_c^1 \\ \mathbf{F}_c^2 \\ \mathbf{F}_s^1 \\ \mathbf{F}_s^2 \end{Bmatrix} = \mathbf{\Phi}_{\boldsymbol{F}}^{in} \begin{Bmatrix} \mathbf{a}_1^+ \\ \mathbf{a}_2^+ \end{Bmatrix} + \mathbf{\Phi}_{\boldsymbol{F}}^{out} \begin{Bmatrix} \mathbf{a}_1^- \\ \mathbf{a}_2^- \end{Bmatrix} ,$$

where

$$\mathbf{\Phi}_{\boldsymbol{F}}^{in} = \begin{bmatrix} \mathbf{\Phi}_{\boldsymbol{F}_c}^{1+} & \mathbf{0} \\ \mathbf{0} & \mathbf{\Phi}_{\boldsymbol{F}_c}^{2+} \\ \mathbf{\Phi}_{\boldsymbol{F}_s}^{1+} & \mathbf{0} \\ \mathbf{0} & \mathbf{\Phi}_{\boldsymbol{F}_s}^{2+} \end{bmatrix} \quad \text{and} \quad \mathbf{\Phi}_{\boldsymbol{F}}^{out} = \begin{bmatrix} \mathbf{\Phi}_{\boldsymbol{F}_c}^{1-} & \mathbf{0} \\ \mathbf{0} & \mathbf{\Phi}_{\boldsymbol{F}_c}^{2-} \\ \mathbf{\Phi}_{\boldsymbol{F}_s}^{1-} & \mathbf{0} \\ \mathbf{0} & \mathbf{\Phi}_{\boldsymbol{F}_s}^{2-} \end{bmatrix} .$$

Rearranging in terms of ingoing and outgoing waves from the wave representations from above, Equation 35 takes the form

$$\left[\mathbf{D}_{ii}^j \mathbf{R}_q \mathbf{\Phi}_{\boldsymbol{Q}}^{in} - \mathbf{T}_r \mathbf{R}_f \mathbf{\Phi}_{\boldsymbol{F}}^{in}\right] \begin{Bmatrix} \mathbf{a}_1^+ \\ \mathbf{a}_2^+ \end{Bmatrix} = \left[\mathbf{T}_r \mathbf{R}_f \mathbf{\Phi}_{\boldsymbol{F}}^{out} - \mathbf{D}_{ii}^j \mathbf{R}_q \mathbf{\Phi}_{\boldsymbol{Q}}^{out}\right] \begin{Bmatrix} \mathbf{a}_1^- \\ \mathbf{a}_2^- \end{Bmatrix} . \tag{36}$$

Combining the continuity condition, Equation 33, and equilibrium condition, Equation 36, one obtains the following matrices

$$\mathbf{C}^{+} = \begin{bmatrix} \mathbf{D}_{ii}^{j}\mathbf{R}_q\mathbf{\Phi}_{\boldsymbol{Q}}^{in} - \mathbf{T}_r\mathbf{R}_f\mathbf{\Phi}_{\boldsymbol{F}}^{in} \\ \mathbf{\Phi}_{c}^{in} \end{bmatrix} \quad \text{and} \quad \mathbf{C}^{-} = \begin{bmatrix} \mathbf{T}_r\mathbf{R}_f\mathbf{\Phi}_{\boldsymbol{F}}^{out} - \mathbf{D}_{ii}^{j}\mathbf{R}_q\mathbf{\Phi}_{\boldsymbol{Q}}^{out} \\ \mathbf{\Phi}_{c}^{out} \end{bmatrix}.$$

The scattering matrix is found by solving the equation

$$\mathbf{s} = [\mathbf{C}^{-}]^{-1}\mathbf{C}^{+} \ . \tag{37}$$

Multiplying Equation 36 by the block matrix $\mathbf{L}$ of the left eigenvectors of the form

$$\mathbf{L} = \begin{bmatrix} \mathbf{\Psi}_{\boldsymbol{Q}_c}^{1-} & \mathbf{\Psi}_{\boldsymbol{Q}_s}^{1-} & \mathbf{0} & \mathbf{\Psi}_{\boldsymbol{Q}_c}^{1-} \\ \mathbf{0} & \mathbf{0} & \mathbf{\Psi}_{\boldsymbol{Q}_s}^{2-} & \mathbf{\Psi}_{\boldsymbol{Q}_c}^{2-} \end{bmatrix}$$

the scattering matrix is finally found by

$$\mathbf{s} = [\mathbf{L}\mathbf{C}^{-}]^{-1}\mathbf{L}\mathbf{C}^{+} \ . \tag{38}$$

4. Numerical results

In this section, numerical examples are presented to demonstrate the hybrid method developed for two-dimensional structures. All the plates are considered to be flat isotropic plates in the (x-y) plane. They are semi-infinite in the x direction and infinite in the y direction with thickness $h = 3 \times 10^{-3}$m. All plates have the same material properties: $\rho = 2700\text{kg m}^{-3}$, $E = 0.71 \times 10^{11}\text{Nm}^{-2}$, $\nu = 0.28$. A segment with $L_x = L_y = 3 \times 10^{-3}$m is meshed using one SOLID45 element from the ANSYS software package; SOLID45 is 8-noded with three translational dofs for each node. The mesh has been chosen according to the analytical dispersion curves for these plates. For convenience, the same mesh density was then used for the solid elements representing the joints. In the following, all properties and dimensions are in SI units.

4.1. Line joint result

The first example is for two isotropic plates to confirm that the approach has been implemented correctly and to validate the method against expected results.

The joint is considered to have the same material properties as the plates and the same type of FE has been used. The configuration of this structure is shown in Figure 4.

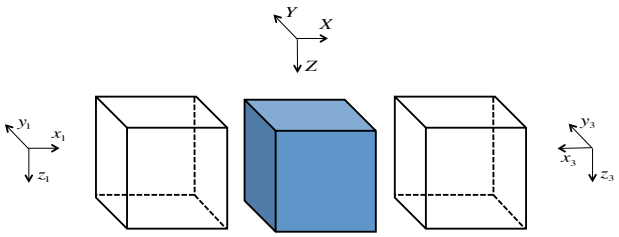

Figure 7: Two semi-infinite plates in the x direction and a joint with infinite length in the y direction and finite length in the x direction. The joint is modelled by a single solid element.

First, the WFE method, as described in section 2, is applied for each plate, and the WFE predictions of the wavenumbers of all the propagating waves are computed. Since the plates are isotropic, the analytical values of the wavenumbers [4, 5] can be calculated as well. A comparison between the analytical values and the ones computed by the WFE method show good agreement and validates the implementation of the WFE method. For general validation and comparison examples of the WFE method concerning the wavenumbers in two-dimensional structures see [11]. The big advantage of WFE method though, is that the WFE method is also applicable for more complicated structures, such as laminates, for which no analytical expression for the wavenumbers can be found.

The hybrid FE/WFE approach allows the computation of the reflection and transmission coefficients of the joint. By using the scattering matrix and the wavemodes the power reflection and transmission coefficients can be calculated by Equation 17.

For normal incidence plane waves, i.e, waves propagating along the x-axis, i.e., $\theta = 0°$ and for different frequencies, perfect transmission (transmission ratio = 1) for bending-to-bending (B-to-B) waves is shown in Figure 8a. The power reflection ratio between bending type waves is zero.

a) b)

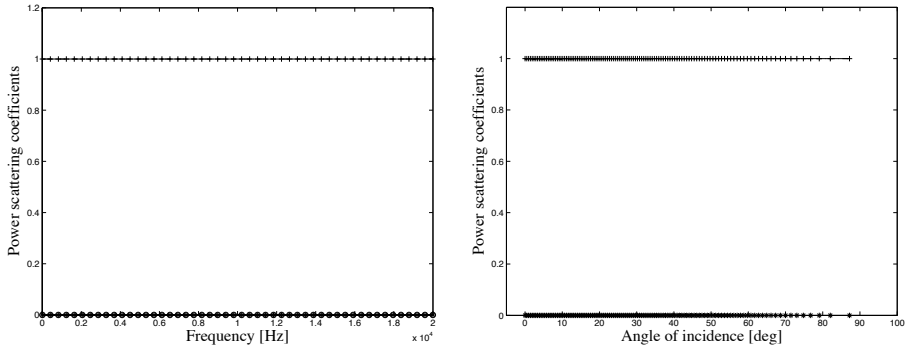

Figure 8: Power reflection and transmission coefficients in case of plates with a joint as in Figure 7. "−+", transmission for B-to-B, "−∗", reflection for B-to-B, "−.", sum of power scattering coefficients for normal incidence versus frequency (Figure 8a) and for different incidence angles at 1kHz (Figure 8b).

One can also investigate the influence of the angle of incidence on the reflection and transmission. Figure 8b shows the power reflection and transmission coefficients for bending-to-bending reflection and transmission at 1kHz with respect to the incidence angle range $(0°, 90°)$. For identical plates perfect transmission occurs at all frequencies and at all angles of incidence with no wave mode conversion taking place.

The third curve, identified in the caption of Figure 8, represents the sum of all the power scattering coefficients for an incoming bending type wave. In this particular case, since perfect transmission occurs this curve coincides with the one for the transmission coefficient for B-to-B and is therefore not visible.

4.2. Lap joint results

This section includes the numerical results which correspond to a joint configuration as in subsection 3.2. This configuration could represent a simple approximation for overlapped bonded plates. The bonded area between the two plates is assumed to be infinitely stiff, massless and of negligible thickness.

Hence the nodes on the overlapped section are coincident in the two plates. For this lap joint case, two different types of joints have been chosen.

4.2.1. First type of lap joint

First the joint is considered as in Figure 9. This joint is modelled by using two elements which are the same ANSYS elements, i.e., SOLID45, and with the same material properties as the plates.

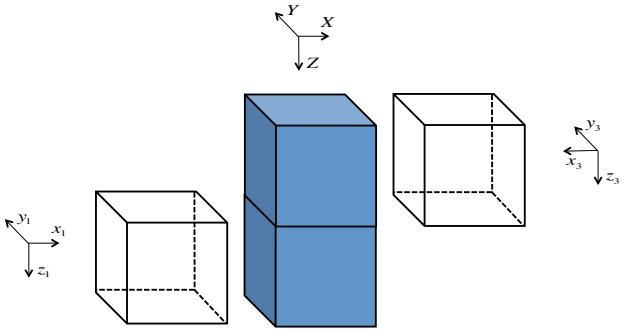

Figure 9: Two plates in an offset where the joint is modelled by two elements.

In a more general sense the joint could also have different properties than the plates. Alternatively the plates could be different from each other or the joint could comprise two elements with different material properties. For the sake of a better understanding of the results, in this article, the material properties are kept the same for all elements. In this case, where there are interface and non-interface nodes between the plates and the joint, as described in subsection 3.2, attention needs to be paid with respect to the ordering and matching of the wavemodes.

Figure 10 shows the reflection and transmission coefficients for a bending type incident wave with respect to the frequency and with respect to the angle.

Close to 0 Hz frequency most of the power of the incident bending type wave propagating in the "Plate 1" is transmitted through the joint into waves of the same type and only an insignificant part of it is reflected or transmitted to other wave types, see Figure 10a. As the frequency increases though, the power

a) b)

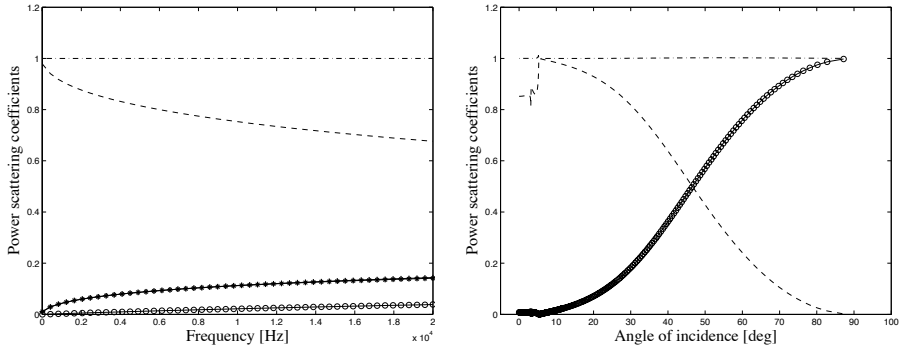

Figure 10: Reflection and transmission coefficients in case of two bonded plates with a joint as in Figure 9. "−−", transmission for B-to-B, "−∘", reflection for B-to-B, "−+", transmission for B-to-A, "−∗", reflection for B-to-A, "−.", sum of all power scattering coefficients for normal incidence versus frequency (Figure 10a) and for different incidence angles at 3kHz (Figure 10b). The curves "−+" and "−∗" are in exact agreement.

is transferred to other wave types as well. For example, one can see that energy is transferred to reflected and transmitted axial type waves (B-to-A). These two curves coincide and therefore are not very well distinguishable in Figure 10a.

In Figure 10b the reflection and transmission coefficients between two bending type waves show that as the angle of incidence is increasing more energy is transferred to reflected waves than to transmitted at a frequency 3kHz. The singularities around $\theta \approx 3$ and $\theta \approx 5$ degrees correspond to the critical angle for the axial and shear type waves. Beyond these angles no propagating waves of these types are generated by an incident bending type wave. At an incidence angle $\theta \approx 90°$, which corresponds to wave propagation in the y direction, ie. grazing incidence, the reflection ratio is 1 and the transmission ratio 0 as expected.

Due to the conservation of energy and as a validation of the computations, both Figures 10a and 10b show that the summation of the power reflection and transmission coefficients for all propagating waves is always unity for lossless

systems.

4.2.2. S-shaped type of joint

The second type of joint in the case of two bonded plates is constructed by using four elements as shown in Figure 11. This joint includes more nodes than the previous one. Therefore, for the needs of the procedure of matching the interface nodes, the extra nodes need to be condensed by using static or dynamic condensation. The rest of the analysis remains the same as for the previous joint and follows subsection 3.2.

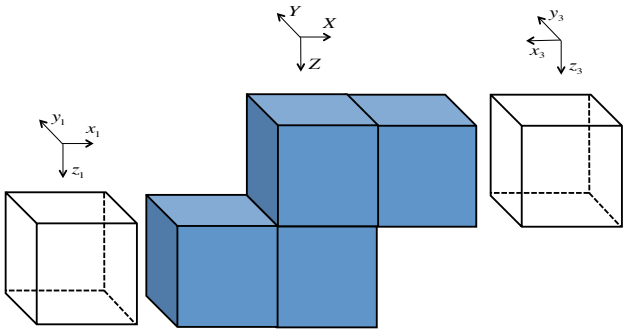

Figure 11: Two plates in an offset where the joint is modelled by four elements.

For both configurations of the lap joint the results in Figure 10 and in Figure 12 look almost identical. There is only a small difference in the reflected power of the bending type waves. When the frequency is increasing the condensation starts having an affect on the approximation. This can be observed in both figures of the reflection coefficient, the one with respect to the frequency and the other with respect to the angle. In the case of the larger joint the reflection at high frequencies is greater than in the case of the smaller joint.

4.3. L-shaped joint results

Another very common type of structure of joined plates in engineering includes two plates in a 90 degrees angle. Depending on the type of joint one

a) b)

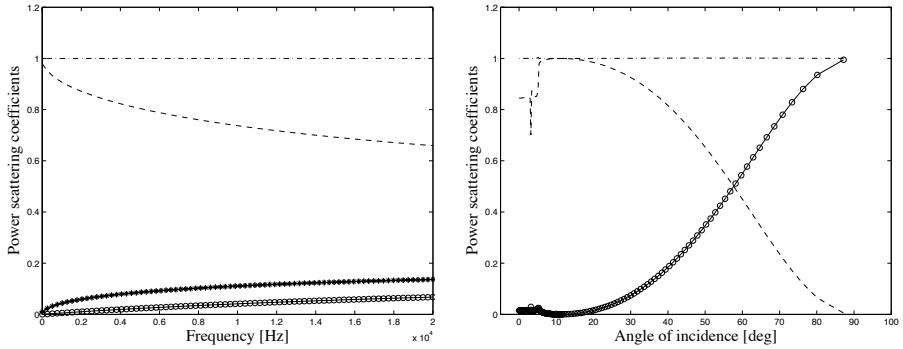

Figure 12: Power reflection and transmission coefficients in case of two bonded plates with a joint as in Figure 11. "−−", transmission for B-to-B, "−∘", reflection for B-to-B, "−+", transmission for B-to-A, "−∗", reflection for B-to-A, "−.", sum of all power scattering coefficients for normal incidence versus frequency (Figure 12a) and for different incidence angles at 3kHz (Figure 12b). The curves "−+" and "−∗" are in exact agreement.

is considering, the hybrid FE/WFE approach follows either the formulation of subsection 3.2 or of subsection 3.3.

4.3.1. Single solid element joint

In the simplest case the joint is of finite length along the x direction, infinitely extended along the y direction and is modelled by the same ANSYS element as the plates, Figure 13. The plates are considered to be semi-infinite and be connected along the y-axis.

The difference in this case compared to the previous examples is that there are nodes on the joint which belong to both plates, i.e., common nodes. This case adds an extra equation to be solved for the continuity condition, i.e. Equation 32.

The results concerning the reflection and transmission coefficients in Figure 14a show that for frequency around 0 Hz and an incident bending type

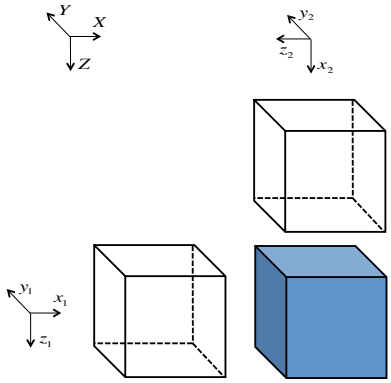

Figure 13: Two plates forming an L-shaped structure where the joint is modelled by a single solid element.

wave, the power is divided into transmitted and reflected power for outgoing waves of the same type. As the frequency increases, the power in the reflected bending wave decreases and the power difference is transferred to other wave types, such as the transmitted axial and reflected wave. The power carried by the shear type waves still remains negligible. Therefore it is chosen not to be shown on the graph, although it is included in the summed power calculation.

Singularities as in subsection 4.2 related to the critical angle around 3 and 5 degrees are observed in Figure 14b. The critical angle depends on the material properties of the plates and not on the configuration of the structure, therefore one sees that for fixed frequency it always occurs at the same angle.

4.3.2. L-shaped type of joint

For the second case, a larger joint is chosen, see Figure 15. For this scenario the interface between the joint and the plates is separate and there are no common nodes. In order to define this joint though many nodes are needed which in an early stage are condensed, in order to make the matching of the interface nodes easier.

The results in Figure 16 are comparable and similar with those in Figure 14.

a) b)

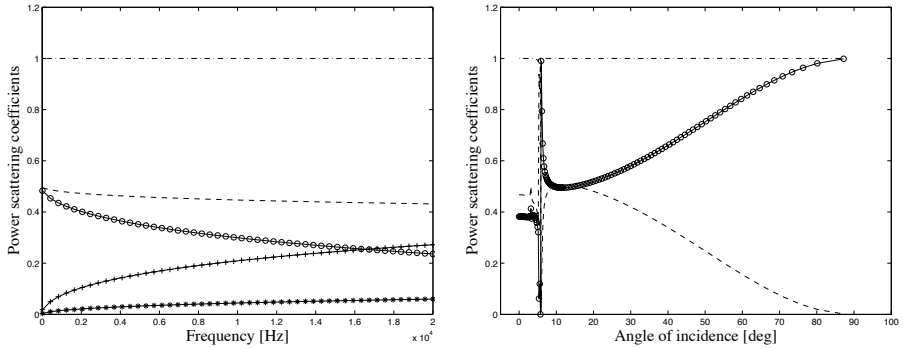

Figure 14: Power reflection and transmission coefficients in case of two plates in 90 degrees angle with the joint as in Figure 13. "−−", transmission for B-to-B, "−∘", reflection for B-to-B, "−+", transmission for B-to-A, "−∗", reflection for B-to-A, "−.", sum of all power scattering coefficients for normal incidence versus frequency (Figure 14a) and for different incidence angles at 3kHz (Figure 14b).

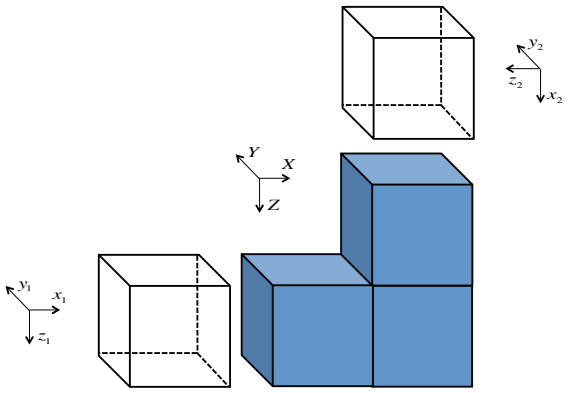

Figure 15: Two plates forming an L-shaped structure where the joint is modelled by three solid elements.

The only difference observed is related to the reflected power in the bending type waves when the frequency increases. The power is greater in the case of the larger joint than for the joint modelled by a single element, since with the

a) b)

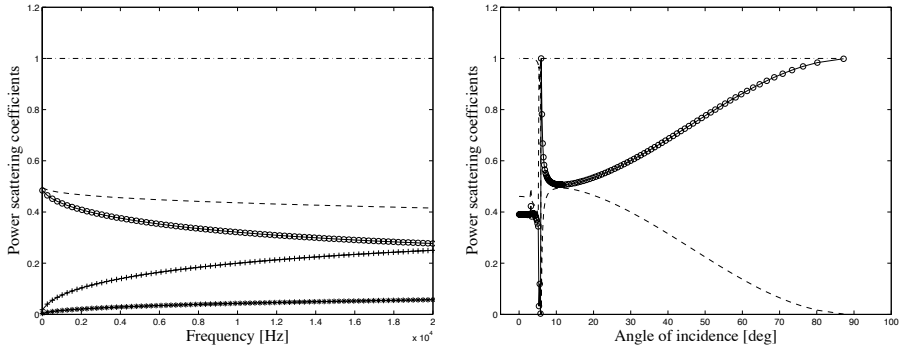

Figure 16: Power reflection and transmission coefficients in case of two plates in 90 degrees angle with a joint as in Figure 15. "−−", transmission for B-to-B, "−∘", reflection for B-to-B, "−+", transmission for B-to-A, "−∗", reflection for B-to-A, "−.", sum of all power scattering coefficients for normal incidence versus frequency (Figure 16a) and for different incidence angles at 3kHz (Figure 16b).

procedure of static condensation a stiffer joint has been created.

The summation to unity of all the power reflection and transmission coefficients shown is the expected result, due to the law of conservation of energy and due to the fact the numerical instabilities have been solved using the orthogonality conditions through the $\mathbf{\Psi}$ matrices.

Junctions of an arbitrary number of plates which are either coupled through a beam or directly coupled along a line have been previously investigated in [15]. A comparison between the method presented by Heron & Langley (H&L) for the case of two plates at 90 degrees angle and the FE/WFE approach is shown in Figure 17. Due to the fact that the analysis in [15] considers as a propagation angle the complementary angle of the angle θ, Figure 17 includes the power scattering coefficients with respect to the cosine of the angle with respect to the interface, i.e., $\cos(90-\theta)$. In the predictions shown in Figure 17 using the earlier wave approach [15], thin plate theory and line connection has been assumed. For sake of uniformity, the transmission coefficients have been

calculated at frequency 3kHz.

The numerical restrictions during the implementation of the WFE method, as for example by fixing the wavenumber component k_y, explain the differences one can notice at higher angles between the two approaches. The correct critical angles are shown from both approaches, even if the one connection is assumed to be along a line, whereas the other over and along a cross sectional area.

Other numerical differences occur due to the modelling of the plates by using either 3D or 2D elements. More details on the effects of the 3D deformation of the cross section with respect to the frequency can be found in [28]. In particular, it has been shown that the shear strain is important on the dynamic response of the joint and at frequency higher than 2kHz the 3D model and the H&L model show significant discrepancies. At frequency lower than 2kHz, i.e., 500Hz, the authors observed a better agreement of the transmission coefficients between the WFE/FE model and the H&L model, as it is suggested in [28].

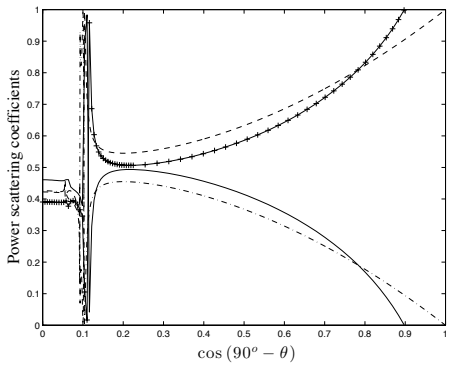

Figure 17: Power reflection and transmission coefficients for different incidence angles at 3kHz in case of two plates in 90 degrees angle. "––", reflection for B-to-B with H&L, "–.", transmission for B-to-B with H&L, "–+", reflection for B-to-B with FE/WFE, "–", transmission for B-to-B with FE/WFE.

4.4. *T-shaped joint results*

The hybrid FE/WFE approach can be further generalised and used in structures comparing three or more plates. Keeping the same principal ideas as in the case of two plates, the only things changing are the size of the matrices and the rotation matrices in order to express the continuity and equilibrium conditions in the global coordinate system.

4.4.1. *Single solid element joint*

In this case, with a joint of the simplest form, the matching of the nodes between the joint and the interface follows subsection 3.3.

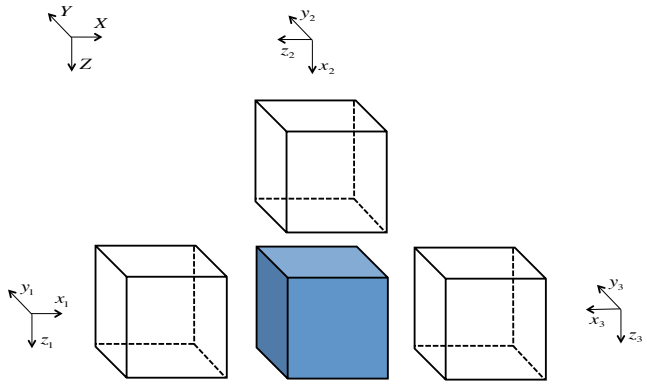

Figure 18: Three plates forming a T-shaped structure where the joint is modelled by a single solid element.

Since there are three connected plates and the incident wave is chosen to propagate from the left hand side plate ("Plate 1") then the joint gives rise to reflected waves, transmitted waves to the vertical plate ("Plate 2") and transmitted waves to the right hand side plate ("Plate 3").

In Figure 19a the reflection and transmission coefficients for an incident bending type wave is shown. By inspection for this model, below 500Hz the power of the bending type wave is mainly reflected to another bending type wave or transmitted to "Plate 2" or to "Plate 3" in the same type of wave. As the frequency increases a significant part of the reflected power is transferred

a) b)

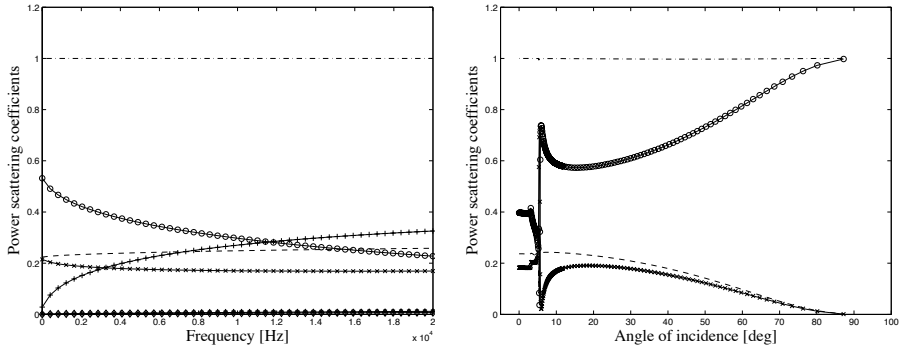

Figure 19: Power reflection and transmission coefficients in case of three plates in a T-shaped structure with a joint as in Figure 18. "−∘", reflection for B-to-B, "−−", transmission for B-to-B from Plate 1 to 2, "−x", transmission for B-to-B from Plate 1 to 3, "−+", transmission for B-to-A from Plate 1 to 2, "−∗", reflection for B-to-A, "−.", sum of all power scattering coefficients for normal incidence versus frequency (Figure 19a) and for different incidence angles at 3kHz (Figure 19b).

to the axial wave propagating in "Plate 2" and the transmitted power in the third plate decreases. The contribution of the bending wave to the other types of waves remains negligible.

Figure 19b shows again numerical singularities around the critical angles and the transmission ratio in "Plate 2" is higher than in "Plate 3".

5. Conclusion

In this article the structures under consideration comprised two or more isotropic plates which are either overlapping or they form an angle between them, such as an L-shaped or a T-shaped type of joint. Analytical models exist for the cases of plates connected in a line with a joint comprised of plates or a beam, but in case of a lap joint or for connections along the cross-section, the hybrid FE/WFE approach becomes a very useful tool. It can, using solid

elements, incorporate the full three dimensional deformation and wave types. In order to apply the hybrid FE/WFE approach and find the scattering properties of the joint one has the possibility to consider different type of joints made of different numbers of elements. The joint is modelled using standard FE and one needs to pay attention only on matching the nodes at the interfaces between the joint and the plates. Through continuity and equilibrium conditions, the power reflection and transmission ratios can be calculated and provide valuable knowledge regarding the wave propagation. With the numerical results it has been shown that, the type of the interface indicates the method which needs to be applied but does not influence significantly the final result.

Acknowledgments

The authors gratefully acknowledge the funding of the European Commission through the Industry-Academia Partnerships and Pathways - Marie Curie Actions under the project MHiVec: "Mid-to-High Frequency Modelling of Vehicle Noise and Vibration" (Project Number 612237). Special thanks to Dr. Niels Søndergaard for implementing the approach in [15] and providing the data for the graph in Figure 17.

References

[1] R. H. Lyon, R. G. DeJong, Theory and Applications of Statistical Energy Analysis, 2nd Edition, Butterworth-Heinemann, Boston, 1995.

[2] G. Tanner, Dynamical energy analysisdetermining wave energy distributions in vibro-acoustical structures in the high-frequency regime, Journal of Sound and Vibration 320 (45) (2009) 1023 – 1038.

[3] D. Chappell, D. Löchel, N. Søndergaard, G. Tanner, Dynamical energy analysis on mesh grids: A new tool for describing the vibro-acoustic response of complex mechanical structures, Wave Motion 51 (4) (2014) 589 – 597, innovations in Wave Modelling.

[4] K. F. Graff, Wave Motion in Elastic Solids, Dover Publications Inc., New York, 1975.

[5] L. Cremer, M. Heckel, B. A. T. Petersson, Structure-Borne Sound, 3rd Edition, Springer, 2005.

[6] B. R. Mace, D. Duhamel, M. J. Brennan, L. Hinke, Finite element prediction of wave motion in structural waveguides, Journal of the Acoustical Society of America 117 (5) (2005) 2835 – 2843.

[7] D. Duhamel, B. R. Mace, M. J. Brennan, Finite element analysis of the vibrations of waveguides and periodic structures, Journal of Sound and Vibration 294 (1-2) (2006) 205 – 220.

[8] L. Houillon, M. Ichchou, L. Jezequel, Wave motion in thin-walled structures, Journal of Sound and Vibration 281 (3-5) (2005) 483 – 507.

[9] M. Maess, N. Wagner, L. Gaul, Dispersion curves of fluid filled elastic pipes by standard fe models and eigenpath analysis, Journal of Sound and Vibration 296 (1-2) (2006) 264 – 276.

[10] J.-M. Mencik, M. Ichchou, Wave finite elements in guided elastodynamics with internal fluid, International Journal of Solids and Structures 44 (7-8) (2007) 2148 – 2167.

[11] B. R. Mace, E. Manconi, Modelling wave propagation in two-dimensional structures using finite element analysis, Journal of Sound and Vibration 318 (4-5) (2008) 884 – 902.

[12] E. Manconi, The wave finite element method for 2-dimensional structures, Ph.D. thesis (2008).

[13] E. Manconi, B. R. Mace, Wave characterization of cylindrical and curved panels using a finite element method, Journal of the Acoustical Society of America 125 (1) (2009) 154 – 163.

[14] J. M. Renno, B. R. Mace, Calculating the forced response of two-dimensional homogeneous media using the wave and finite element method, Journal of Sound and Vibration 330 (24) (2011) 5913–5927.

[15] R. S. Langley, K. Heron, Elastic wave transmission through plate/beam junctions, Journal of Sound and Vibration 143 (1990) 241–253.

[16] I. Bosmans, T. Nightingale, Modeling vibrational energy transmission at bolted junctions between a plate and a stiffening rib, Journal of Acoustical Society of America 109 (3) (2001) 999–1010.

[17] S. Walsh, R. White, Vibrational power transmission in curved beams, Journal of Sound and Vibration 233 (3) (2000) 455 – 488.

[18] P. Mees, O. Vermeir, Structure-borne sound transmission at elastically connected plates, Journal of Sound and Vibration 166 (1) (1993) 55 – 76.

[19] P. Craven, B. Gibbs, Sound transmission and mode coupling at junctions of thin plates, part i: Representation of the problem, Journal of Sound and Vibration 77 (3) (1981) 417 – 427.

[20] P. Craven, B. Gibbs, Sound transmission and mode coupling at junctions of thin plates, part ii: Parametric survey, Journal of Sound and Vibration 77 (3) (1981) 429 – 435.

[21] C. Hopkins, Statistical energy analysis of coupled plate systems with low modal density and low modal overlap, Journal of Sound and Vibration 251 (2) (2002) 193 – 214.

[22] C. Hopkins, Experimental statistical energy analysis of coupled plates with wave conversion at the junction, Journal of Sound and Vibration 322 (12) (2009) 155 – 166.

[23] J. M. Renno, B. R. Mace, Calculation of reflection and transmission coefficients of joints using a hybrid finite element/wave and finite element approach, Journal of Sound and Vibration 332 (9) (2013) 2149–2164.

[24] Y. Waki, B. R. Mace, M. J. Brennan, Numerical issues concerning the wave and finite element method for free and forced vibrations of waveguides, Journal of Sound and Vibration 327 (1-2) (2009) 92–108.

[25] W. Zhong, F. Williams, On the direct solution of wave propagation for repetitive structures, Journal of Sound and Vibration 181 (3) (1995) 485 – 501.

[26] W. Zhong, F. Williams, A. Y. T. Leung, Symplectic analysis for periodical electro-magnetic waveguides, Journal of Sound and Vibration 267 (2) (2003) 227 – 244.

[27] S.-K. Lee, B. Mace, M. Brennan, Wave propagation, reflection and transmission in curved beams, Journal of Sound and Vibration 306 (35) (2007) 636 – 656.

[28] V. Zalizniak, Y. Tso, L. Wood, Waves transmission through plate and beam junctions, International Journal of Mechanical Sciences 41 (7) (1999) 831 – 843.